Paul W.H. Voorhaar Stress Engineering

VORTEX GENERATION IN WATER WAVES

PROPAGATING OVER A SUBMERGED RECTANGULAR DIKE

Date: Vr 09-Jul-1999
Time: 17:56:37

Project: UITDIEPEN VAN TOEKOMSTPERSPECTIEF
Jobnr: PV1999

ABSTRACT:

The unsteady, two-dimensional Navier-Stokes equations and the exact free surface boundary conditions have been solved to simulate the flow separation and the vortex generation in water waves propagating over a submerged rectangular dike. The computed water surface elevations at different locations have been compared with experimental ones to verify the accuracy of the numerical method. The vorticity of the flow near the dike are calculated from the numerical velocity fields. Effects of the Keulegan-Carpenter number on the vortices is investigated. The wave forces on the dike are also determined. It was found that the wave force nearly reaches its highest value when the wave crest is above the dike.

KEY WORDS:
Submerged dike, higher harmonics, vortex generation, Keulegan-Carpenter number.

P.W.H. Voorhaar

REFERENCES:

M.Isaacson "Wave Forces on Rectangular Caissons" (1979)
C.C. Mei and J.L. Black "Scattering of Surface waves by Rectangular Obstacles in Waters of Finite depth" (1969)

REV	BY	DATE	DESCRIPTION	CHECKED	PROJECT APPROVAL	THIRD PARTY APPROVAL
0	PVo	Vr 09-Jul-1999	First Issue			

STATUS CODE	DOCUMENT NUMBER	REVISION	STATUS
A Preliminary for information only B For review C Authorized for construction	**SP99002**	**0**	**A**

Proceedings of the Ninth (1999) International Offshore and Polar Engineering Conference
Brest, France, May 30-June 4, 1999

ISBN 1-880653-39-7 (Set); ISBN 1-880653-42-7 (Vol. III); ISSN 1098-6189 (Set)

Vortex Generation in Water Waves Propagating Over a Submerged Rectangular Dike

C.M. Dong and C.J. Huang
National Cheng Kung University
Tainan, Taiwan, China

ABSTRACT

The unsteady, two-dimensional Navier-Stokes equations and the exact free surface boundary conditions have been solved to simulate the flow separation and the vortex generation in water waves propagating over a submerged rectangular dike. The computed water surface elevations at different locations have been compared with experimental ones to verify the accuracy of the numerical method. The vorticity of the flow near the dike are calculated from the numerical velocity fields. Effects of the Keulegan-Carpenter number on the vortices is investigated. The wave forces on the dike are also determined. It was found that the wave force nearly reaches its highest value when the wave crest is above the dike.

KEY WORDS: Submerged dike, higher harmonics, vortex generation, Keulegan-Carpenter number.

INTRODUCTION

In previous approaches, impermeable seawalls or revetments were very often used to prevent beach erosion. However, the incident waves are reflected from the seaward faces of these structures and ultimately cause structural subsidence. In new techniques, the seaward surfaces of the seawall are covered with riprap or made of step-faces to reduce the reflection. The offshore breakwater has also received great attention in the past few decades. Offshore breakwaters are used along shorelines to reduce the wave energy impinging upon beaches. A submerged dike has been used as one of the general types of offshore breakwater.

When a wave propagates over a submerged dike, it breaks ocassionally as the wave crest meets the top of the dike. In addition, the flow separates from the structure and vortices are generated near the dike. A major effect of the vortices is aggravation of the erosion of the sea bed at the toe of the dike. Furthermore, the great rate of shear strain associated with the vortices can seriously damage the fabric of the submerged structure. Hence it is important for ocean engineers to understand the dynamics of vortex shedding from the submerged dike.

Previous studies on water waves over a submerged obstacle have been mainly concerned with determining the reflection and transmission characteristics of water waves. To date, most of the studies on this subject concentrated on the nonlinear effects of the waves. The problems mentioned above were typically treated using potential theory, which assumes that the flow is irrotational. Within the framework of linear theory, the transmission and reflection coefficients have been studied by Takano (1960) and Mei and Black (1969). They found that the reflection coefficient decreases monotonically as the height of the dike decreases. The nonlinear interaction of water waves with a submerged rectangular dike has been studied recently by Massel (1983), Rey et al. (1992), Grue (1992), Driscoll et al. (1993), and Ohyama and Nadaoka (1993). Massel (1983) employed the potential theory combining nonlinear free surface boundary conditions to study the generation of free wave and bound wave. The variations in the wave energy flux between the leading and the trailing sections of the dike has been studied by Grue (1992) using the Boussinesq equation. The boundary element method has also been applied to solve the Laplace equation and the nonlinear free surface boundary conditions to simulate the nonlinear deformation of water waves (e. g. Driscoll et al., 1993; Ohyama and Nadaoka, 1993). A comparison of these computational results with experimental data indicates that the potential theory fails to accurately reproduce the experimental results on the lee side of the dike. The reason is due to the presence of vortices in the real flow field, which cannot be predicted using potential theory.

Recently, flow visualization techniques have been employed to observe the vortex movement in the wave field. Rey et al. (1992) observed the phenomenon of vortex generation in water waves over a

submerged dike using dye. Ting and Kim (1994) conducted laboratory experiments to investigate the flow separation and vortex generation induced by waves propagating over a submerged rectangular dike. Velocity measurements were obtained using a two-component laser-Doppler anemometer (LDA). The formation and growth of the vortices shedding from a submerged rectangular dike in waves was studied by Petti et al. (1994) using the PIV method. The phenomenon of vortex generation can be observed by the dye method, but the quantitative properties of the vortices cannot be determined. Although the LDA can measure the velocities accurately, it is very time consuming to construct the overall velocity field as it measures only the instantaneous velocity at one location.

In order to simulate the real flow fields around submerged dikes, the Navier-Stokes equations and the exact free surface boundary conditions have to be solved. A few numerical models have been proposed for the problem of water waves interacting with a submerged dike. Huang and Sue (1998) simulated the flow field induced by waves propagating over a submerged rectangular dike using the VOF (volume of fluid) numerical method. Huang and Dong (1999) studied the wave deformation and the vortex generation in water waves propagating over a submerged dike, in which the effects of different parameters on the wave transformation and vortex generation were studied systematically. However, in the above mentioned papers the behaviors of vortices were not discussed in detail. In this paper, we will extend our previous study on the interaction of water waves and a submerged dike and concentrate on the behavior of the vortices. The effects of K-C number on the vortices were studied.

GOVERNING EQUATIONS AND BOUNDARY CONDITIONS

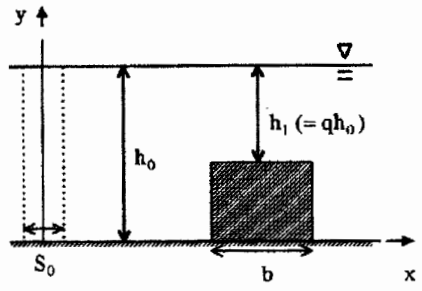

Fig. 1 Schematic diagram of a submerged rectangular dike.

The vortex generation in water waves passing over a submerged dike was investigated in this study. A schematic diagram of a rectangular dike is shown in Fig. 1. A piston-type wavemaker with stroke S_o is located at x=0 and generates the incident waves. The still water depth is h_o. The width of the dike is b. The shallow water depth above the dike is $h_1 (= qh_o,\ 0 < q < 1)$. For an incompressible, viscous fluid, the dimensionless continuity equation in the Cartesian coordinate system is

$$\frac{\partial u}{\partial x} + \frac{\partial v}{\partial y} = 0 \qquad (1)$$

and the Navier-Stokes equations are given by

$$\frac{\partial u}{\partial t} + u\frac{\partial u}{\partial x} + v\frac{\partial u}{\partial y} = -\frac{\partial p}{\partial x} + \frac{1}{R_e}\left(\frac{\partial^2 u}{\partial x^2} + \frac{\partial^2 u}{\partial y^2}\right) \qquad (2)$$

and

$$\frac{\partial v}{\partial t} + u\frac{\partial v}{\partial x} + v\frac{\partial v}{\partial y} = -\frac{\partial p}{\partial y} + \frac{1}{R_e}\left(\frac{\partial^2 v}{\partial x^2} + \frac{\partial^2 v}{\partial y^2}\right) \qquad (3)$$

where u and v are the horizontal and vertical velocity components, t is the time, p is the hydrodynamic pressure, and R_e is the Reynolds number, defined as $R_e = u_o h_o / \upsilon$. Where υ is the kinematic viscosity of the fluid, and u_o is the velocity-amplitude of the wavemaker, which moves back and forth with a velocity of $u = u_o \sin \omega t$. In this case, u_o and h_o were used to non-dimensionalize the velocity and length, while $t_o = h_o / u_o$ was chosen to non-dimensionalize the time.

The kinematic free surface boundary condition states that fluid particles at a free surface remain on the free surface, and can be expressed as

$$\frac{\partial \eta}{\partial t} + u\frac{\partial \eta}{\partial x} = v \qquad (4)$$

where $\eta = \eta(x,t)$ is the location of the free surface.

The dynamic free surface boundary condition requires that, along the free surface boundary, the normal stress is equal to the atmospheric pressure and the tangential stress is zero. These conditions were expressed by Huang et al. (1998) as the following

$$p_o = \frac{\eta}{F_r^2} + \frac{2[1 + (\frac{\partial \eta}{\partial x})^2]}{R_e[1 - (\frac{\partial \eta}{\partial x})^2]}\frac{\partial v}{\partial y} \qquad (5)$$

and

$$\frac{\partial u}{\partial y} = -\frac{\partial v}{\partial x} + \frac{4}{(\frac{\partial \eta}{\partial x})^2 - 1}\frac{\partial v}{\partial y}\frac{\partial \eta}{\partial x} \qquad (6)$$

where $p_o = p(x,\eta)$ is the hydrodynamic pressure at the free surface and F_r is the Froude number, defined as $F_r = u_o / \sqrt{g h_o}$.

In the numerical computations, Eq. (5) was used to determine the pressure at the free surface and Eq. (6) was used to extrapolate the horizontal velocity at the free surface from the flow domain. The vertical velocity component v was then calculated from the continuity equation using the known velocity component u, obtained from Eq. (6).

The downstream boundary condition requires that, at a large distance from the wavemaker, the wave is outgoing without reflection. According to the wave equation and continuity equation, we can set

$$\frac{\partial p}{\partial t} + c\frac{\partial p}{\partial x} = 0, \qquad \frac{\partial u}{\partial t} + c\frac{\partial u}{\partial x} = 0, \qquad \frac{\partial u}{\partial x} + \frac{\partial v}{\partial y} = 0 \qquad (7)$$

where c is the phase speed of the wave and is determined from the dispersion relation. The no-slip boundary condition is imposed on

the channel bottom and the obstacle surface. The initial conditions of the velocities, hydrodynamic pressure, and surface displacements are set at zero at time $t = 0$.

NUMERICAL METHOD

In this study the finite-analytic (FA) method was applied to discretize the unsteady two-dimensional Navier-Stokes equations. In this method, local analytical solutions obtained from the linearized Navier-Stokes equations for the discretized computational elements were incorporated into the numerical method. The FA equations of Equation (2) or (3) are

$$f_p = (C_s f_s + C_n f_n + C_w f_w + C_e f_e + C_t f_p^{n-1}) + C_p S_f \qquad (8)$$

where the coefficient C with different subscripts are the FA coefficients, which relate to the time step and the grid size. The finite-analytic symbols for nonuniform grids are shown in Fig. 2. S_f is the finite difference formulation of ($R_e \partial p / \partial x$) or ($R_e \partial p / \partial y$). A detailed discussion of this numerical method can be found in the .found in the paper of Chen and Patel (1987).

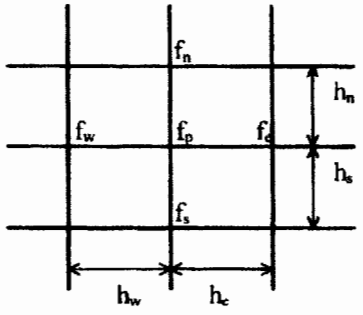

Fig. 2 Symbols used in the present numerical method.

The SIMPLER algorithm developed by Patankar (1980) was used to calculate the coupled velocity and pressure fields. A staggered numerical grid was used. The Marker and Cell method (MAC) and its modified version SUMMAC were used in combination to calculate the free surface boundary. For a detailed description of the numerical procedure one is referred to Huang et al. (1998).

In the numerical model, the Eulerian grid system was used, which means that the form and size of the computational grids were fixed. However, the computational domain near the wavemaker changed as the wavemaker moved back and forth. In the computation, the grids in the neighborhood of the wavemaker were so arranged that the boundary of the computational domain matched the location of the wavemaker. The numerical results shown in the following were calculated with dimensionless Δx and Δy equal to 0.1, except for the region near the submerged obstacle where the finest grid size Δx and Δy was 0.05. The increment of dimensionless time was chosen to be 0.001.

NUMERICAL RESULTS AND DISCUSSION

(i) Verifications

The numerical results were compared with the experimental data obtained by Driscoll et al. (1993) to verify the accuracy. The experiments were conducted in a wave tank of 30-m long, 0.6-m wide, and 1-m deep. A submerged rectangular dike was placed 7-m away from the wavemaker. The still water depth was $h_o = 0.5$ m. The rectangular dike was 0.79-m width and 0.38-m high (i.e. $q = 0.24$). The incident wave height H_i and period T were 2.5 cm and 1.7 sec, respectively. The wave gages were placed at locations 0.72 m and 1.92 m away from the trailing edge of the dike. Fig. 3 shows a comparison of the numerical and experimental results of the wave profiles at several stations and times. The results obtained by Driscoll et al. (1993) using BEM model are also presented in the figure for comparison. We noted from Fig. 3 that our numerical results are in good agreement with the experimental data and are better than those obtained by BEM model. The accuracy of the spatial evolution of the first three harmonic wave amplitudes are also verified before we can proceed with a study of the behavior of the vortices. To make this comparison, numerical computations were carried out with the same experimental conditions as that of Ting and Kim (1994). In their experiments the still water depth was 60.96 cm, the incident wave height and period were 5.85 cm and 4.0 sec. Fig. 4 shows the comparison of the numerical and experimental results of the spatial evolution of the first three harmonic amplitudes. The wave amplitudes were normalized by the amplitude of the incident wave, and the coordinate x was normalized with respect to the width of the submerged dike which was located from x/b=0 to x/b=1. We can see from Fig. 4 that the computed amplitudes of each harmonic agreed favorably with the measured amplitudes.

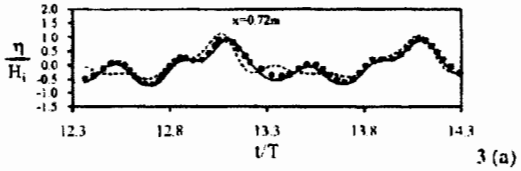

3 (a)

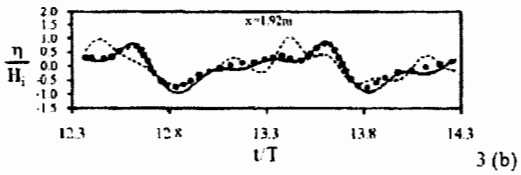

3 (b)

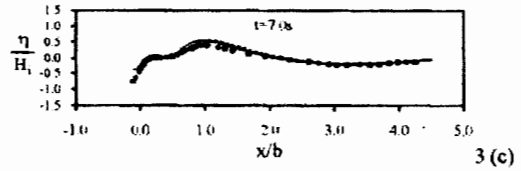

3 (c)

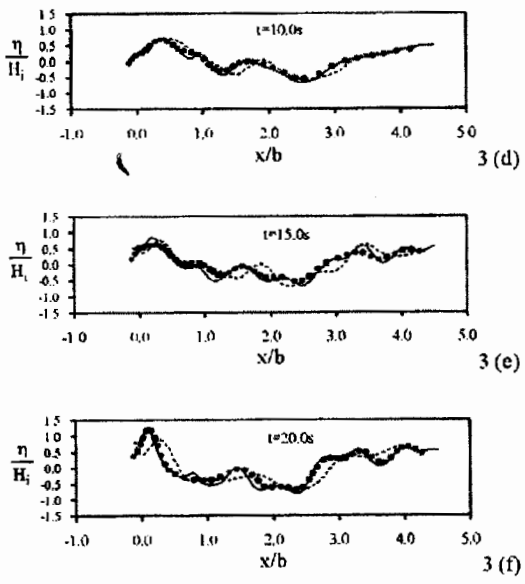

Fig. 3 Wave profiles at several stations and times for monochromatic incident waves with $H_{in} = 2.5$ cm, $T = 1.7$ s, $q = 0.24$ passing over a rectangular dike. (●) Experimental data (Driscoll et al., 1993); (—) Results of present numerical model : (—)BEM (Driscoll et al , 1993).

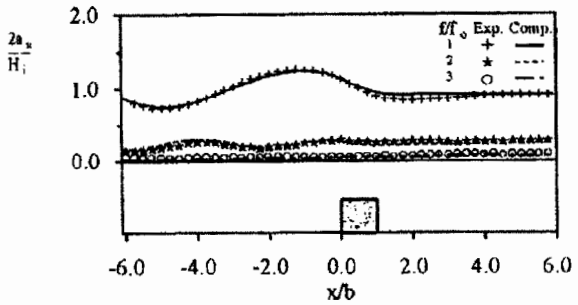

Fig. 4 Spatial evolution of the first, second and third harmonic wave amplitudes; $h_0 = 60.96$ cm , $T = 4.0$ s , $H_i = 5.85$ cm .

(ii) Numerical conditions

The circulation, Γ, induced by waves passing over a submerged dike can be related to the following variables:

$$\Gamma = f(H_i, L, h_0, h_1, b, \rho, \mu, g, t) \qquad (9)$$

where H_i is the wave height, L is the wavelength of the incident waves, h_0 is the still water depth, h_1 is the water depth above the dike, b is the width of the dike, ρ is the density and μ is the dynamic viscosity of the water, g is the gravitational acceleration, and t is the time. Physical reasoning leads to one particular choice of dimensionless groups as

$$\frac{\Gamma}{H_i c} = f\left(\frac{H_i L^2}{h_0^3}, \frac{H_i L}{h_0^2}, \frac{h_1}{h_0}, \frac{b}{h_0}, \frac{H_i cL}{\upsilon h_0}, \frac{t}{T}\right) \qquad (10)$$

in which $\Gamma / H_i c$ is the normalized circulation, $H_i L^2 / h_0^3$ is the Ursell number which represents the nonlinearity of the incoming waves, $H_i L / h_0^2$ is the Keulegan-Carpenter number in shallow water, h_1 / h_0 is the water depth ratio, b / h_0 is the aspect ratio of the dike, $H_i cL / (h_0 \upsilon)$ is the Reynolds number for viscous wave fields according to Huang and Dong (1999), and T is the incident wave period. The Keulegan-Carpenter number (abbreviated as K-C No.) is interpreted as the ratio of maximum displacement of a fluid particle from its neutral position to the body length, and is an important parameter in determining the formation and development of vortices in the flow. When the still water depth remains constant, the Ursell number and the Reynolds number increase with the Keulegan-Carpenter number. Hence, we only have chosen the independent parameters, namely the K-C No., to study their effects on the behavior of vortices. The conditions for the numerical simulation are summarized in Table 1. In cases 1 to 4 the K-C numbers increase from 0.48 to 2.13, while the corresponding Ursell numbers increase from 3.33 to 32.52. Also to note that in all of the numerical simulations, we have confined ourselves to nonbreaking waves.

Table 1. Numerical conditions

Variable	Case 1	Case 2	Case 3	Case 4
h_0(m)	0.25	0.25	0.25	0.25
H_i(cm)	1.7	3.2	3.35	3.5
L(m)	1.75	2.17	3.00	3.81
T(s)	1.25	1.5	2.0	2.5
$H_i L^2 / h_0^3$	3.33	9.64	19.30	32.52
$H_i L / h_0^2$	0.48	1.11	1.61	2.13
$H_i cL / h_0 \upsilon$	1.9×10^5	4.3×10^5	6.3×10^5	8.4×10^5
b(m)	0.25	0.25	0.25	0.25
q	0.5	0.5	0.5	0.5

(iii) Vortices generated by wave propagation

Fig. 5 shows the variation in the flow fields with respect to different wave phases for Case 4. We noted from Fig. 5 that as the wave trough propagates over the left edge of the dike (t/T=0), a flow separation occurs at the left corner of the dike. As the wave trough approaches the right edge of the dike (t/T=3/24), due to the large horizontal velocity in the negative x-direction, a flow separation with reattachment is formed at the right corner of the dike and it develops into a separation bubble (t/T=6/24). At the same time, a counter-clockwise vortex is generated on the weather side of the dike. As

the wave trough propagates downwards, both the separation bubble and the counter-clockwise vortex diminish gradually (t/T=9/24). Similarly, as the wave crest propagates over the left edge of the dike (t/T=12/24), due to the large horizontal velocity near the crest, flow separation with reattachment is formed at the left corner of the dike and it develops to a separation bubble (t/T=15/24). As the wave crest propagates downstream (t/T=18/24), the horizontal velocities of the flow particles on the lee side of the dike are accelerated. Due to the strong velocity gradient, a clockwise vortex is generated at this region. This vortex seems to be stronger than the vortex on the weather side. Meanwhile the separation bubble diminishes in the decelerated flow and it eventually disappears at t/T=21/24. From t/T=18/24 to t/T=21/24 the clockwise vortex continues to grow until the horizontal velocity changes direction.

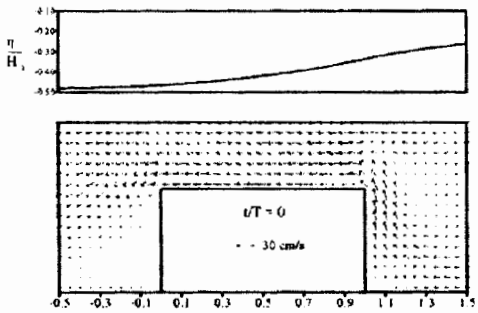

5 (a)

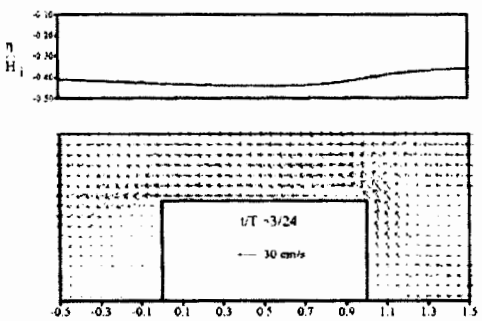

5 (b)

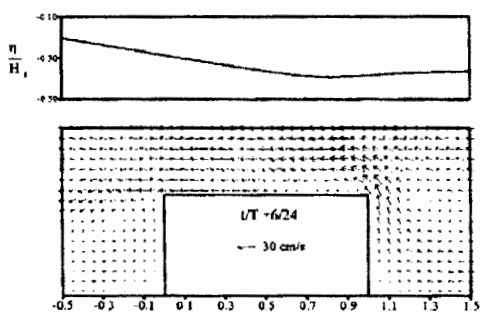

5 (c)

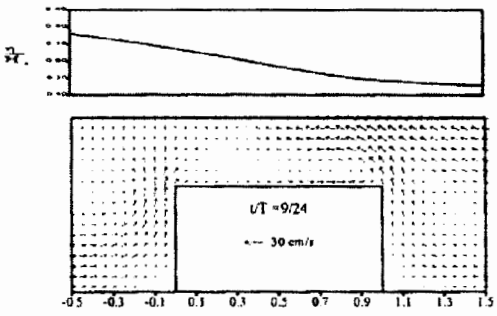

5 (d)

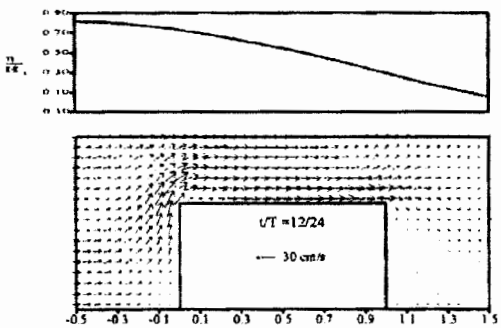

5 (e)

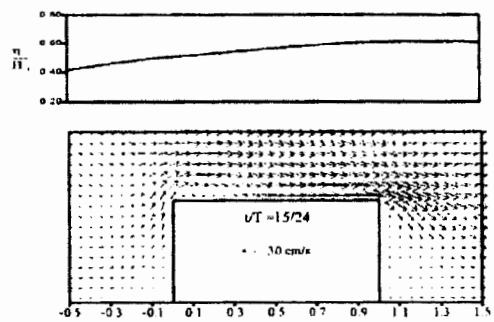

5 (f)

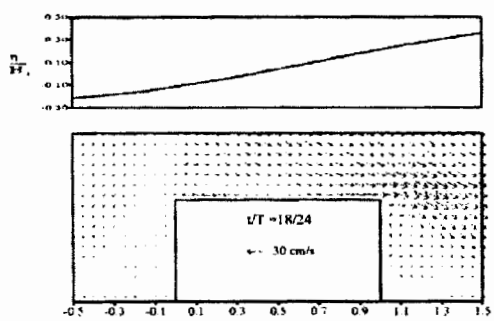

5 (g)

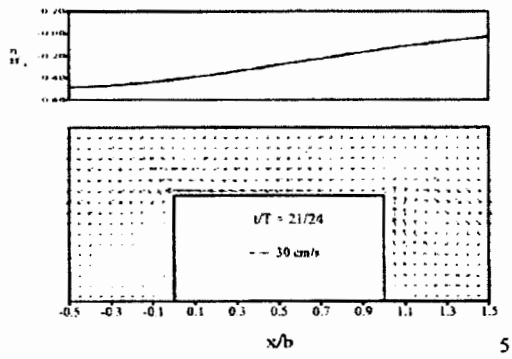

5 (h)

Fig. 5 Surface elevations and velocity fields at different times for Case 4; H_i = 3.5 cm, T = 2.5 s.

(iv) Circulation

Since the wave motion is periodic, the pattern and strengths of the vortices induced by the waves are also periodic. The variations in vortex strength on the lee and weather sides of the dike were studied in terms of circulation, which by definition is the surface integral of the vorticity. The vorticity, defined as $(\partial u/\partial y - \partial v/\partial x)$, was calculated from the velocity field using the finite-difference scheme. The clockwise and counter-clockwise circulation's were then determined separately by integrating the negative and the positive vortices over the region of vortex motion, which ranged from very near the bottom to the free surface. The circulation is said to be counterclockwise if the integral is positive, and to be clockwise if the integral is negative. In the determination of the circulation, the vortices within the boundary layer were not taken into account, because in this study we were mainly interested in the circulation in the main flow region.

The normalized circulation for Cases 2 to 3 are shown in Figs. 6 to 7. In these figures, part (a) shows the variation in circulation on the weather side of the dike within one wave cycle, while part (b) shows the variation on the lee side of the dike. The symbols t, st, c, and sc in part (a) denote the phase situation of the wave above the left edge of the dike. Here t indicates the wave trough, st the still water level after the trough, c the wave crest, and sc the still water level after the crest. The symbols on part (b) denote the phase situation of the wave above the right edge of the dike. From part (b) of Fig. 6 to Fig. 7 we noted that the clockwise circulation on the lee side becomes maximum when the still water level (sc) is above the right edge of the dike. This can be explained as follows: when the still water level (st) is above the right edge of the dike, the clockwise vortex obtains a continuous supply of energy until the next still water level (sc) arrives. In a similar manner, we can explain why the counterclockwise circulation in part (a) of Fig. 6 to Fig. 7 becomes maximum when the wave phase above the left edge of the dike lies between the trough (t) and the still water level after trough (st). The clockwise circulation, shown in part (a) of Fig. 6 to Fig. 7, indicates that in addition to the main counterclockwise circulation, there is also positive vorticity existing on the weather side of the dike. This idea applies also to part (b).

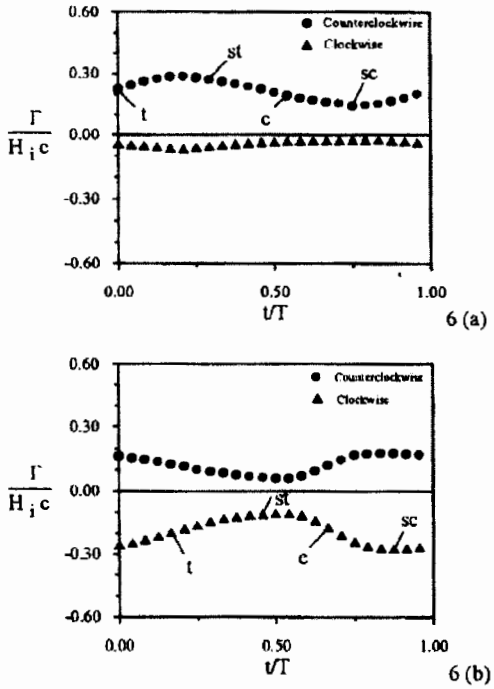

6 (a)

6 (b)

Fig. 6 Variation in circulation within one wave cycle for Case 2; H_i = 3.2 cm, T = 1.5 s. (a) weather side. (b) lee side.

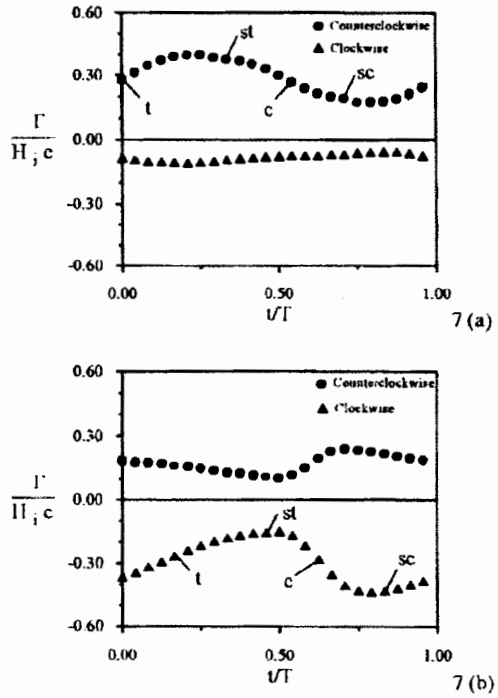

7 (a)

7 (b)

Fig. 7 Variation in circulation within one wave cycle for Case 3; H_i = 3.35 cm, T = 2.0 s. (a) weather side. (b) lee side.

(v) The effects of K-C number on the circulation

The effect of the K-C number on the maximum value of the circulation is shown in Figs. 8 (a) and (b). We can see from Fig. 8 (a) and (b) that the circulation increases with the K-C number. This is because the maximum displacement of a fluid particle becomes greater, if the K-C number increases. This greater particle velocity can extend the region and strength of the vortex.

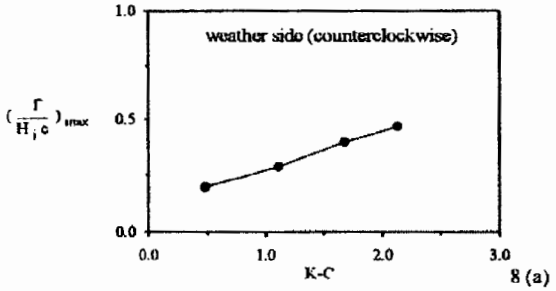

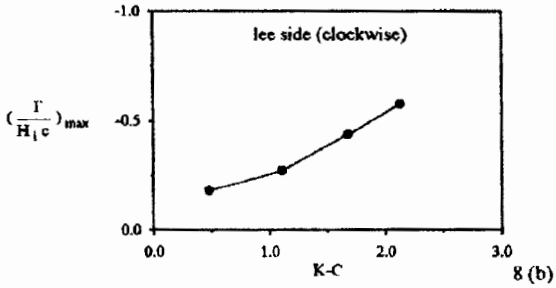

Fig. 8 Variation in the maximum value of circulation with K-C number.

(vi) Wave forces on the submerged dike

Determination of the wave force on the ocean structure is very important for the design of the structures. In this section the wave forces acting on the left and the right walls of the dike are discussed. The results for Case 2 to Case 3 are shown in Fig. 9 to Fig. 10, respectively. The wave forces are normalized with the hydrostatic force $\frac{1}{2}\gamma(1-q^2)h_0^2$ on the lateral wall of the dike. In comparison Fig. 6 to Fig. 7 with Fig. 9 to Fig. 10 we can see that the maximum wave force on the left wall of the dike occurs when the wave crest is nearly above the left edge of the dike. This indicates that the influence of vortex shedding on the wave force is not noticeable as water waves passing over the dikes. Similar conclusion has also been reported by Mogridge and Jamieson (1976) and Isaacson (1979). We note also that wave force on the left wall becomes larger as the Ursell number increases. The wave force on the right wall is weaker than that on the left wall (Fig. 9a to 10a), because a part of incident wave is reflected from the submerged structure. The relative width of the submerged structure (b/L) becomes smaller as the Ursell number increases, this makes the phase lag between the right-side force and the left-side force in Case 3 shorter than the Case 2. This phenomenon can also be found from the phase diagrams of the two forces (see Fig. 10 (b)). If the phase diagram is flat, the phase shift between two forces is small, and the phase lag becomes larger, if the diagram is rounder.

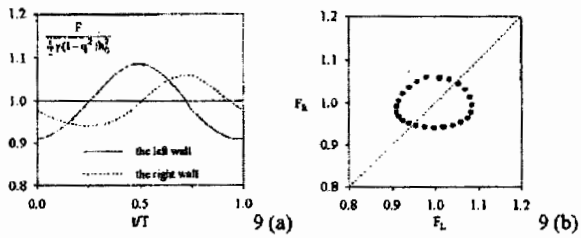

Fig. 9 Wave forces for Case 2; H_i = 3.2 cm, T = 1.5 s. (a) time series diagram. (b) phase diagram of two forces.

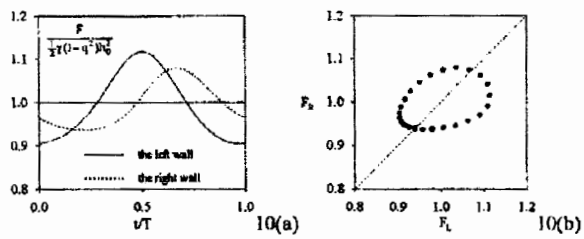

Fig. 10 Wave forces for Case 3; H_i = 3.35 cm, T = 2.0 s. (a) time series diagram. (b) phase diagram of two forces.

CONCLUSIONS

A numerical scheme has been developed to solve the Navier-Stokes equations and the exact free surface boundary conditions. The vortex generation as water waves passing over a submerged rectangular dike has been investigated by the numerical model. The following major conclusions can be drawn from this investigation:

1. The computed wave profiles agree favorably with the experimental observations, indicating that the present numerical model is accurate.
2. The clockwise circulation on the lee side of the dike is maximum, when the still water level after crest (sc) is above the right edge of the dike. The counterclockwise circulation on the weather side of dike becomes maximum when the wave phase above the left edge of the dike lies between the trough (t) and the still water level after trough (st).
3. The circulation and the separation zone increase with the Keulegan-Carpenter number. The clockwise circulation on the lee side is larger than the counter-clockwise circulation on the weather side as the K-C number increases.

4. The wave force on the left wall of the dike is almost maximum when the wave crest is above the left edge of the dike. The influence of vortex generation on the wave forces is not noticeable.

The total force acting on the dike may also be required in the real engineering applications. To determine this force, the shear stresses on the dike wall must also be calculated. If the velocity profiles in the boundary layer are known, the distribution of shear stresses on the wall can be calculated. To achieve this, refined grids near the dike are necessary. As we know from the present study and from Huang and Dong's paper (1999) that, the flow separations occurs at the leading and trailing edges of the dike when waves passing over it. A detailed study of the viscous flow near the dike will include the interaction of flow separation and the wave-induced boundary layer. However, this is beyond the scope of the present study and will be left as our future research topic.

ACKNOWLEDGMENT

This research was supported by the National Science Council, Taiwan, under Contract No. NSC 87-2621-P-006-032.

REFERENCES

Chen, HC and Patel, VC (1987). "Laminar Flow at the Trailing Edge of a Flat Plate," *AIAA J.*, Vol. 25, pp 920-928.

Driscoll, AM, Dalrymple, RA, and Grill, ST (1993). "Harmonic Generation and Transmission Past a Submerged Rectangular Obstacle," *23rd Coastal Eng. Conf.*, pp 1142-1152.

Grue, J (1992). "Nonlinear Water Waves at a Submerged Obstacle or Bottom Topography," *J. Fluid Mech.*, Vol. 244, pp 455-476.

Huang, CJ and Dong, CM (1999). "Wave Deformation and Vortex Generation in Water Waves Propagating over a Submerged Dike," to be published in *Coastal Eng.*.

Huang, CJ, Zhang, EC, and Lee, JF (1998). "Numerical Simulation of Nonlinear Viscous Wavefields Generated by a Piston-Type Wavemaker," *J. Eng. Mech.*, Vol. 124, pp 1110-1120.

Huang, RR and Sue, YC (1998). "Numerical Simulation on Nonlinear Interaction of Water Waves with Submerged Obstacles," *Proc. Flow Modeling and Turbulence Measurements VII, Taiwan, ASCE*, pp 545-554.

Isaacson, M (1979). "Wave Forces on Rectangular Caissons," *Proc. Civil Engineering in the Oceans IV, San Francisco, ASCE*, pp 161-171.

Mei, CC and Black, JL (1969). "Scattering of Surface Waves by Rectangular Obstacles in Waters of Finite Depth," *J. Fluid Mech.*, Vol. 38, pp 499-511.

Mogridge, GR and Jamieson, WW (1976). "Wave Forces on Square Caissons," *15th Coastal Eng. Conf.*, pp 2271-2289.

Massel, SR (1983). "Harmonic Generation by Waves Propagation over a Submerged Step," *Coastal Eng.*, Vol. 7, pp 357-380.

Ohyama, T and Nadaoka, K (1993). "Modeling the Transformation of Nonlinear Waves Passing over a Submerged Dike," *23rd Coastal Eng. Conf.*, pp 526-539.

Ohyama, T and Nadaoka, K (1994). "Transformation of a Nonlinear Wave Train Passing over a Submerged Shelf without Breaking," *Coastal Eng.*, Vol. 24, pp 1-22.

Patankar, SV (1979). "A Calculation Procedure for Two-Dimensional Elliptic Situations," *Numerical Heat Transfer*, Vol. 2.

Petti, M., Quinn, PA, Liberatore, G, and Easson, WJ (1994). "Wave Velocity Field Measurement over a Submerged Breakwater," *24th Coastal Eng. Conf.*, pp 525-539.

Rey, V, Belzons, M, and Guazzelli, E (1992). "Propagation of Surface Gravity Waves over a Rectangular Submerged Bar," *J. Fluid Mech.*, Vol. 235, pp 453-479.

Takano, K. (1960). "Effects d'un Obstacle Parallelipipedique sur la Propagation de la Houle," *Houille Blanche*, Vol. 2, pp 247-267.

Ting, FCK and Kim, YK (1994). "Vortex Generation in Water Waves Propagating over a Submerged Obstacle," *Coastal Eng.*, Vol. 24, pp 23-49.